JCTC Journal of Chemical Theory and Computation

ARTICLE

pubs.acs.org/JCTC

Analysis of Mammalian Histidine Decarboxylase Dimerization Interface Reveals an Electrostatic Hotspot Important for Catalytic Site Topology and Function

Aurelio A. Moya-García,[†,‡,∥] Daniel Rodríguez-Agudo,[†,∥,⊥] Hideyuki Hayashi,[§] Miguel Angel Medina,[†,‡] José Luis Urdiales,[†,‡] and Francisca Sánchez-Jiménez*[,†,‡]

[†]Departamento de Biología Molecular y Bioquímica, Facultad de Ciencias, Campus de Teatinos, Universidad de Málaga, Málaga, Spain

[‡]CIBER de Enfermedades Raras (CIBERER), Málaga, Spain

[§]Department of Biochemistry, Osaka Medical College, Takatsuki, Osaka 569-8686, Japan

ABSTRACT: Selective intervention of mammalian histidine decarboxylase (EC 4.1.1.22) could provide a useful antihistaminic strategy against many different pathologies. It is known that global conformational changes must occur during reaction that involves the monomer−monomer interface of the enzyme. Thus, the dimerization surface is a promising target for histidine decarboxylase inhibition. In this work, a rat apoenzyme structural model is used to analyze the interface of the dimeric active HDC. The dimerization surface mainly involves the fragments 1−213 and 308−371 from both subunits. Part of the overlapping surfaces conforms each catalytic site entrance and the substrate-binding sites. In addition, a cluster of charged residues is located in each overlapping surface, so that both electrostatic hotspots mediate in the interaction between the catalytic sites of the dimeric enzyme. It is experimentally demonstrated that the carboxyl group of aspartate 315 is critical for the proper conformation of the holoenzyme and the progression of the reaction. Comparison to the available information on other evolutionary related enzymes also provides new insights for characterization and intervention of homologous l-amino acid decarboxylases.

1. INTRODUCTION

Mammalian histidine decarboxylase (HDC) is a pyridoxal 5′-phosphate (PLP)-dependent enzyme that is responsible for the biosynthesis of histamine. This biogenic amine is involved in several physiological responses (e.g., immune responses, gastric acid secretion, neurotransmission, etc.), and consequently, it has been implicated in many different human pathologies such as anaphylaxis, peptic ulcers and other inflammatory responses, basophilic leukemias, osteoporosis, schizophrenia, rare diseases such as histidinemia (ORPHA2157), and mast cell related rare diseases such as the different mastocytoses (ORPHA98292, ORPHA66646, ORPHA2467, ORPHA98848, ORPHA98849, and ORPHA98850). In spite of the importance of these diseases, HDC has not been fully characterized. Thus, most of the current antihistaminic strategies tend to interfere with histamine reception by target cells (i.e., histamine receptors) rather than with histamine synthesis in histamine-producing cells. However, the recent development of HDC knock-out animals suggests that HDC activity is itself important for the development and proliferation of the cells that produce it,[1] indicating that selective intervention of histamine synthesis could be a straightforward pharmacological strategy for some of the histamine-related pathologies.

Mature histidine decarboxylase purified from mammalian tissues has been reported as a dimer where each monomer (53−58 kDa) is processed from a carboxy-elongated 74 kDa precursor.[1,2] It has been demonstrated that the first 476 residues of the protein can support the enzymic activity.[3] We have characterized the catalytic mechanism of a recombinant version of a carboxy-truncated form of the rat enzyme (fragment 1−512, also named HDC 1/512),[4] which has kinetic constants similar to the mature enzyme purified from rodent tissues.[2] We studied the rate-limiting step with atomic detail.[5] We have observed that the Stokes radius of the protein is modified during catalysis, indicating that local changes in the catalytic site of mammalian histidine decarboxylase affect its global conformation by a rearrangement of the dimerization surface.[6] A flexible region (within residues 330−360) has been proven to participate[7−10] in the conformational changes of the catalytic site neighborhood after substrate binding, and we have established the role of this region in the increased stability of the enzyme on substrate uptake.[11] These results have highlighted the importance of dimerization for the enzymic activity of this protein and consequently implicate dimerization as a potential target for selective inhibition of this mammalian enzyme. Thus, we focus on the characterization and analysis of the intermonomer interaction surface of this enzyme.

The computational analysis in the present work revealed that an electrostatic hotspot, with contributions of the same cationic and anionic residues from both monomers, is located between the two catalytic sites of the homodimer. Residue D315 plays an important role in the stabilization of the electrostatic hotspot and the right active site conformation. This hypothesis was experimentally tested by direct mutagenesis strategies, biophysical measurements, and enzymic activity determinations.

2. MATERIALS AND METHODS

2.1. Structure Preparation. In order to investigate the hotspot contribution to both the electrostatic properties and monomer

Received: December 1, 2010
Published: May 13, 2011

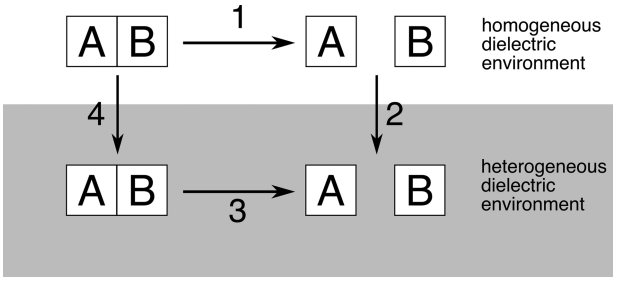

Figure 1. Thermodynamic cycle for calculation of binding free energy. The binding free energy is calculated from the transfer free energies of the protein from a homogeneous dielectric environment to a heterogeneous dielectric environment.

binding, we generated structural models for several mutations of rat HDC (rHDC). Taking our previous homology-based model[5] as the wild type enzyme, mutations of selected hotspot residues were performed with PyMOL[12] on each monomer of the homodimeric enzyme.

To define the monomer−monomer interactions surface, water accessibilities of the residues were calculated with the DSSP program,[13] and the proper protonation state at physiological pH and atomic charges were established using the PDB2PQR and PROPKA server and software[14,15] in order to obtain a suitable input structure for electrostatics calculations.

The initial geometry of each system was relaxed using the Steepest Descent algorithm (10 000 energy minimization steps) and the OPLS force field implemented in the DYNAMO library.[16] Each mutated structure was solvated in a 41.8 Å radius sphere of TIP3P explicit water molecules and subjected to Molecular Dynamics (MD) simulations with NAMD[17] and the CHARMM22 protein force field.[18] The systems were heated to 310 K followed by equilibration without restraints using Langevin dynamics to control the temperature. Once equilibrated, coordinates were saved every 10 ps to obtain 20 ns MD trajectories.

2.2. Energy Calculations. Electrostatics binding free energies for the formation of the homodimeric rHDC complex (ΔG^{elec}) were calculated by combining several hypothetical processes in the thermodynamic cycle,[19] depicted in Figure 1. The electrostatic binding free energy is then given by:

$$\Delta G^{elec} = -\Delta G_3 = \Delta G_4 - \Delta G_2 - \Delta G_1$$

Our framework essentially decomposes ΔG^{elec} in terms of transfer free energies from a homogeneous dielectric environment (in which a dielectric constant of 4 is applied to the protein and the solvent) to a heterogeneous dielectric environment with different internal and external dielectric constants (namely, 4 for the protein and 80 for the solvent). In other words, we compute the electrostatic contribution to the binding free energy in terms of solvation and Coulombic electrostatic interaction free energies. The Adaptive Poisson−Boltzmann Solver (APBS)[20] was used to compute the contribution of solvation to ΔG^{elec} by solving the Poisson−Boltzmann equation for the complex and for each component, in both the homogeneous and the heterogeneous dielectric environments. Intermolecular Coulombic contributions to ΔG^{elec} (ΔG_{coul}) are considered in our simulations by computing the change in Coulombic electrostatic energy upon complex formation in a homogeneous dielectric environment (with a dielectric constant of 4), ΔG_1 depicted in Figure 1. Thus

$$\Delta G_{coul} = -\Delta G_1 = \Delta G^{AB} - \Delta G^{A} - \Delta G^{B}$$

Each term in this equation is the sum of pairwise Coulombic interactions among all atoms in the two rHDC monomers or in the rHDC dimer. These terms were calculated with the accessory program Coulomb, from the APBS software. The temperature was 298 K, and the ionic strength equaled 0.15 M in all cases.

Due to the strong dependence of the calculated free energies on the value taken for the protein dielectric constant and the discussion and controversy regarding the most appropriate value of this parameter,[21−23] it is difficult to know whether the calculated ΔG^{elec} accurately represents experimental energies. Therefore, the calculated values for ΔG^{elec} are meaningful only for the comparison of relative complex formations among the wild type enzyme and the mutants studied, so we offer relative binding affinities in terms of $\Delta\Delta G^{elec} = \Delta G^{elec}(\text{mutant}) - \Delta G^{elec}(\text{wt})$, where positive values indicate a decreased binding affinity and negative values indicate an affinity increase caused by the mutation.

2.3. Electrostatic Potential Maps. Electrostatic potential maps were calculated using APBS to solve the Poisson−Boltzmann equation. The protein is centered in a 193 × 193 × 161 grid. A solvent dielectric constant of 80 and a protein dielectric constant of 4 were used for the electrostatic potential map calculations, as they are standard values used by other authors.[24]

2.4. Recombinant HDC Expression and Purification. Direct mutants were generated using the Quickchange system (Promega). The previously reported recombinant pBluescript SK-II plasmid encoding for fragment 1−512 of rat HDC (namely, p1/512.rHDC) was used as the template.[25] The primers used for the different substitutions were the following: D315V, 5′-GGATGATGGTGCACTTT*GTT*TGCACTGGGTTCTGGG-3′ (sense) and its antisense counterpart (the mutated codon is in italic lettering); D315N, equal to the previous ones but AAT and its antisense counterpart are in the respective primers as the mutated codon; and C316A, 5′-GGATGATGGTGCACTTTGAC*GCC*ACTGGGTTCTGGG-3′ (sense) and its antisense counterpart. All mutants were tested using full double-strand sequencing after each subcloning step. Different expression systems have been used throughout this work for the wild-type and the mutant versions. The in vitro expression system was previously described.[25] The purified preparations of the recombinant versions were obtained as described elsewhere.[4] For rapid screening of activities, the mutant enzymes were expressed and purified from recombinant pGEX6P-1 plasmids as mutant versions of the pGEX6P-1/HDC1/512 product, as reported previously.[4] The mutant versions were released from the glutathione S-transferase fusions by treatment with the Pre-Scission TM protease supplied with the kit. The HDC activity assay was carried out by following $^{14}CO_2$ release from [U-$^{14}CO_2$]-labeled L-histidine (American Radiolabeled Chemicals, U. S. A.), as reported elsewhere.[25] Spectroscopic measurements were carried out with the expression product of a recombinant pET11a plasmid encoding for mutant D315N. It was expressed and purified as reported elsewhere for the wild-type enzyme, following three chromatographic steps (Phenyl-Sepharose CL-4B, DEAE interchange, and hydroxyapatite).[4,6] Purity of the final preparations was assessed by Coomassie blue staining and Western blotting. All preparations used in this work had greater than 90% purity. When required, the enzyme was concentrated in different Amycon ultrafiltration systems (cutoff between 10 and 30 kDa) depending on the initial volume. To

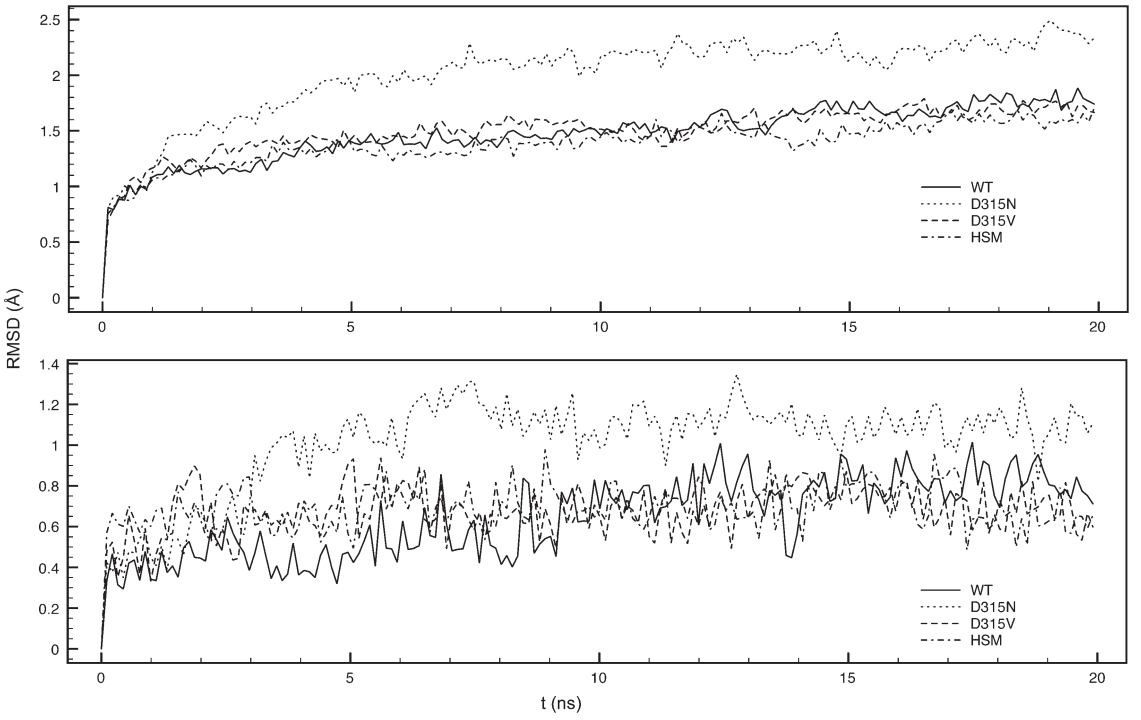

Figure 2. Root-mean-square deviations from the first structure of the MD trajectory for each system studied, for the backbone (upper graph) and hotspot residues (lower graph). WT, wild-type HDC; HSM, hotspot mutant.

avoid interferences with free PLP, the final preparation was gel filtrated in a Sephadex G25 immediately before starting spectroscopic measurements. For the experiments shown in Figures 3 and 4, purified HDC preparations were incubated at room temperature in either the presence or absence of histidine methyl ester (HisOMe) for 60 min. HisOMe and histidine were provided by Sigma-Aldrich (Spain).

2.5. Spectroscopic Measurements. Absorption spectra were measured using a HP8452A diode array spectrophotometer (Hewlett-Packard, U. S. A.). Fluorescence spectra were obtained with a QuantaMaster SE spectrofluorimeter (Photon Technology International Inc., U. S. A.). All spectroscopic measurements were carried out at RT under the same conditions as those described previously.[4]

3. RESULTS AND DISCUSSION

3.1. General Description of the Dimer Interface. Our previous work indicates that the dimerization surface must be involved in conformational changes occurring during catalysis,[6] so we focused our attention on this part of the enzyme. In a close examination of the dimerization surface, we found a cluster of charged residues in each monomer between both catalytic sites. Dimerization and active site conformations were explained previously.[31] This led us to hypothesize that the electrostatic properties of this hotspot would be important in maintaining a proper environment in each active site.

To check putative dramatic reorganizations in the molecular structures after the mutations, we built molecular models for mutations in the hotspot of HDC, and we made molecular dynamics simulations with these versions. Results showed that no major changes or structural reorganization occur in the enzyme as a consequence of the mutations (Figure 2). In fact, backbone root-mean-square deviations from the initial structure are below 2.5 Å during the 20 ns MD trajectory, and root-mean-square deviations in the hotspot are below 1.4 Å for the wild type and mutant models. Thus, the mutations do not seem to cause important rearrangements in the enzymatic structure.

We computed changes in the electrostatic properties of the monomer−monomer interface to address the importance of surface complementarity in enzymatic activity using our homology model of mammalian HDC structure. The major features of the predicted quaternary structure of the mammalian enzyme are (Figure 3) as follows: the dimer presents a 2-fold axial symmetry; the first 100 residues of both polypeptides are intertwined; two catalytic sites are conformed within the dimer interface, involving mainly random coiled fragments of the central polypeptide sequence of both monomers.

Residues taking part in the dimer interface were predicted by calculating the differences in the water accessibility scores of each residue when comparing the monomeric and the dimeric models. Water accessibility values decreasing by more than 12 $Å^2$ after dimerization are the following: S5, Y7, Y10, Q11, K15, M17, V18, Y20, I21, Y24, L25, R31, P35, V37-R43, I46, S48, A50, P54, D55, W57, I60, I64, I68, M69, G71-Q76, Y83, Y84, A86, T88, L93, L94, D96-L98, D100-L105, F107-S111, P113, E117, L118, M120, N121, D124, W125, K128, D134, H139-P141, R151, T152, S154, E155, T157, L158, L161, L162, R165, D180, E181, S182, N185, A186, A190, A192, H197, S198, V200-F213, E225, F243, T251, K308, H313-D315, F331-V333, P335-Y337, R339, H340, N342, V345, T347, M350, I354-R359, W366, F367, R370, S371, E424, K428, F437, I439, P440, and T442. They map the dimerization surface. From these data, it can be deduced that dimerization mainly involves residues of the amino-terminus, up to residue 213, and those between positions 308 and 371 of each monomer. The dimerization surface and the location of the active

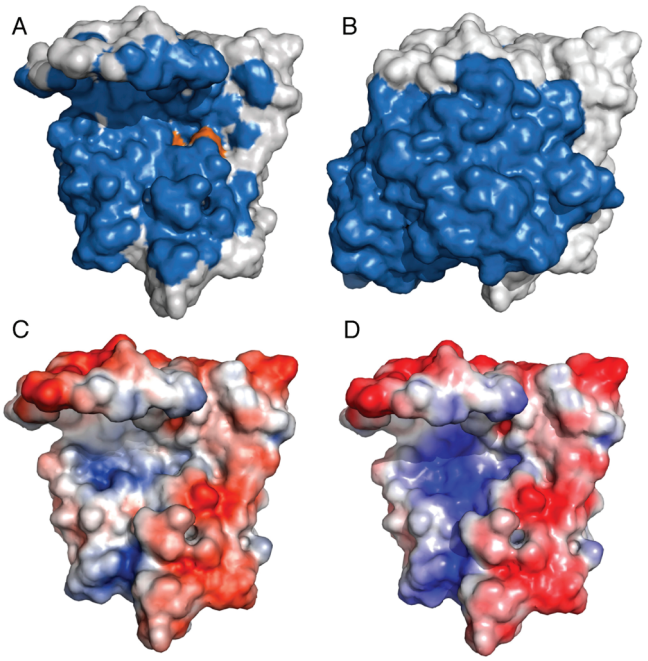

Figure 3. Dimerization surface and electrostatic potential maps. The dimerization surface is shown in dark blue, and the active site is colored in orange, mapped by K308 and H197 (A). Quaternary structure of rHDC: one subunit is colored in dark blue, and the other is colored in white (B). The lower panels show the surface representations of the electric potential, for the wild-type (C) and the hotspot mutant (D). Color range from deep red to deep blue corresponds to the range in values of electrostatic potential from −3.1 to +3.1 kT/e, where k is the Boltzmann constant, T is the absolute temperature, and e is a proton's charge.

site (mapped by K308 and H197) are shown in panel A of Figure 3. K308 is the residue responsible for the covalent PLP binding during internal aldimine formation, and H197 seems to stabilize the pyridine ring of the cofactor, not only in HDC but also in other homologous enzymes.[26−28] Both residues, colored in orange in Figure 3A, indicate the position of the PLP-binding site.

Protein−protein interaction surfaces are geometrically complementary. In nonpermanent complexes, where each component can exist in solution, electrostatic contacts direct protein−protein interaction, while in permanent complexes hydrophobic contacts are dominant.[29] Electrostatic complementarity between interacting proteins is also generally assumed[30] despite the generally low and often unfavorable contribution of electrostatics to the assembly of a complex.[22]

Mammalian HDC is proposed as a homodimer,[31,32] and as can be seen in Figure 3, there is important shape complementarity. Most of the hydrophobic surface of each monomer is quenched during dimerization. Thus, as expected for a permanent complex, hydrophobic contacts direct monomer−monomer interactions. There is only one electrostatic patch on the dimerization surface of each monomer; it is located next to the PLP binding site of the contrary monomer. This electrostatic hotspot is formed by side chains of residues D96, D100, R151, E155, D315, and R359, all of them exposed to the dimer interface and delineating an area of positive potential (Figure 3C), suggesting a way to stabilize negatively charged PLPs in the active sites.

Because both monomers have an identical patch, they must influence the dimer conformation by minimizing direct contact between these areas. We checked the role of this patch in stabilizing the quaternary structure, comparing the electrostatic potential in the dimerization surface of the wild-type enzyme and a mutant in which every residue of the electrostatic hotspot was replaced with valine residues. Results are shown in Figure 3C and D. In the hotspot mutant HDC, the positive electrostatic potential patch is considerably larger than that of the wild type enzyme, in accordance with the net elimination of two negative charges. The hotspot mutant HDC cannot avoid the overlapping of these two electropositive regions. Consequently, the relative binding affinity of the hotspot mutant HDC is $\Delta\Delta G^{elec}$ = 371.518 kcal/mol. This large dimer destabilization indicates that the electrostatic patch contributes to stabilizing the dimeric quaternary structure in mammalian HDC.

3.2. Aspartate 315 is Predicted to Play an Important Structural Role. The fact that the enzyme minimizes an unfavorable monomer−monomer electrostatic interaction, provided that it can maintain a polar environment between the two active sites, points to the idea that the enzyme needs these charges. We focused our attention on residue D315 due to the following observations. This negatively charged residue holds a central position in the electrostatic hotspot, and it is located close to the essential residue K308 (10 Å between both α-carbons). Both K308 and D315 take part in the same random-coiled loop (residues 305−317). In spite of their opposite charges, these two residues could not establish a direct interaction because the aromatic group of F314 (of the same polypeptide) prevents such interactions. Consequently, the orientation of the D315 γ-carboxylate group does not seem to be determined by the secondary structure of the fragment but by polarity of the residues in its surroundings. Only four residues, namely, F314 (monomer A), D315 (monomer A), D315 (monomer B), and F314 (monomer B), separate the two K308 residues of the homodimer. Altogether, these considerations allow us to hypothesize an essential role for the carboxylate group of this residue as a stabilizer of the electrostatic hotspot at its closest part to both catalytic centers. Besides its effect on the electrostatic potential, removal of D315 could also disturb the optimal topology of the catalytic site (mainly K308 orientation) and consequently the PLP-binding to the apoenzyme and subsequently the HDC activity.

3.3. Aspartate 315 is Proven to Be Essential for HDC Activity. We generated computationally and experimentally two different substituted mutants called D315V and D315N. In the former, the acid group moiety was substituted by an uncharged group with a similar volume. The second substitution nullified the positive charge of the group. Both versions, together with the wild 1/512 version, were expressed in vitro and in *E. coli* and were further purified. In all cases, no enzymatic activity was detectable for both D315 mutants by following decarboxylation of radiolabeled histidine, even when both concentrations of the purified dimeric enzyme were higher than 7 μM and 3.2 mM histidine was used.

In order to test whether D315N contributes to establishing a proper quaternary structure, binding free energies were computed for the four systems (Table 1) as described in the Materials and Methods section.

These results indicate that removal, or even amidation, of the carboxylate group at this position has dramatic consequences on the catalytic site structure.

It was necessary to check whether this effect on the active site could be reproduced by mutation of any other residue as close to the catalytic site as D315. This was tested with a C316A mutant. In addition, this residue is one of the most conserved residues in the 308−316 fragment (apart from the essential K308), not only

Table 1. Electrostatic Binding Free Energies of Wild Type and Mutants HDC[a]

	WT	D315N	D315 V	C316 V
ΔG^{elec}	−294.942	−134.669	−161.871	−289.761
$\Delta\Delta G^{elec}$		160.273	133.071	5.181

[a] Reported values (kcal/mol) are calculated as described in the Materials and Methods section: $\Delta\Delta G^{elec} = \Delta G^{elec}(\text{mutant}) - \Delta G^{elec}(\text{wt})$. Positive values indicate a dimer stability decrease, whereas negative values indicate a complex stability increase.

among mammalian HDCs but also in other evolutionarily related enzymes. In contrast to D315 mutants, the C/A substitution, which abolishes any polar interaction of this residue, gave rise to an active HDC with a 66 ± 5% (mean ± SD, $n = 3$) reduction in activity compared to the wild-type 1/512 version. The calculated relative affinity for C316V (Table 1) together with those calculated for the D315 mutants show a direct relationship between electrostatic binding free energy and enzyme activity. We conclude that a proper electrostatic complementarity between both HDC monomers is essential for a proper quaternary structure of the enzyme and thus for the activity. In addition, D315 plays a fundamental role in stabilizing the electrostatic patch that directs monomer−monomer interactions, and it establishes an electropositive environment in the PLP interaction region of each active site.

3.4. Amidation of the D315 Carboxylate Group Is Enough to Alter Catalytic Site Conformation and PLP Binding. Because enzymic activity was followed by CO_2 decarboxylation, the D315 mutants seem to lack the ability to release CO_2 (one of the final products). However, we wanted to further check whether the reaction could at least proceed during its first steps (Michaelis complex and/or external aldimine formation). For PLP-dependent enzymes, this kind of information can be obtained from spectroscopic approaches by analyzing absorption and fluorescence spectra of the cofactor during Michaelis complex and PLP−substrate or PLP−product complex formation.[27,33] In fact, this approach has been used previously for the recombinant wild-type 1/512 version.[4,6] The substrate analog histidine methyl ester (HisOMe) acts as the substrate during the initial steps and reproduces the spectral changes observed with histidine but blocks the reaction in the external aldimine state (PLP-substrate complex). Thus, any HDC enzyme that could accept the substrate (or the analogue) and proceed along any of these steps would change the shape of its spectrum.

Absorption spectra of wild-type HDC (Figure 4) reproduced those reported previously.[4] They reveal a major enolimine tautomeric form for the holoenzyme (maximum at 335 nm) and a low percentage of the complex in the ketoenamine tautomeric form (maximum at 420 nm). However, the spectra of the analogue-untreated mutant enzyme were very different to those of the free wild-type holoenzyme and HisOMet could induce no major shift when added up to the final 5 mM concentration. The main absorption bands of D315N are those centered at 360−370 nm and at 470−480 nm. Unusual spike peaks are also found at 380 and 450 nm. Additionally, the shallow valley between the two peaks suggests the presence of absorption peak(s) in this region (around 430 nm). At a glance, the overall shape of the absorption spectrum of D315N suggests that the two main bands correspond to those of the wild-type enzyme. If this is the case, the 360 and 480 nm absorption bands could reflect the enolimine and ketoenamine structures of the Schiff base, which are 30−50 nm red-shifted by some conformational or environmental factors. As an approach to identify the components of these absorption peaks, we measured the fluorescence (Figure 5A) and excitation (Figure 5B) spectra because different structures of PLP Schiff bases show distinctive fluorescence spectra.[27,33]

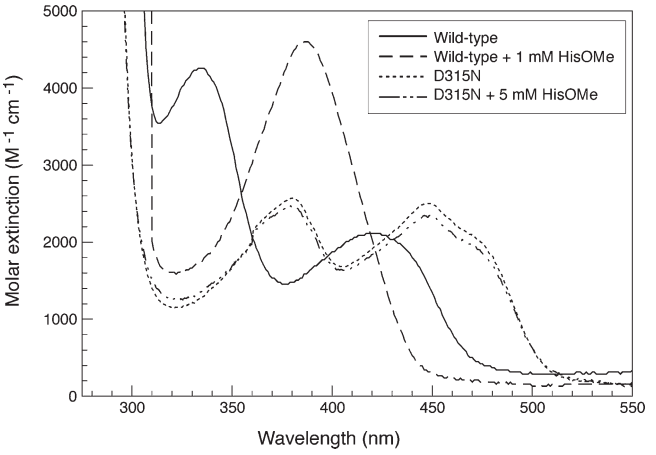

Figure 4. Absorption spectra of the HDC 1/512 wild-type and its mutant D315N in the absence or the presence of the substrate analog histidine methyl ester (HisOMe). Spectra of purified and gel-filtered wild-type 1/512 and D315N HDC were recorded before and 1 h after HisOMe addition.

With excitation at 360, 380, 430, 450, and 480 nm, fluorescence was observed with maximum emission wavelengths at 434, 454, 507, 527, and 556 nm, respectively. That is, the emission wavelengths were generally 74−77 nm longer than the excitation wavelength. The observed fluorescence spectra with variable maximum emission wavelengths indicate that the two main absorption bands are each composed of multiple absorption transitions. These transitions may correspond to distinct species. Alternatively, they may be considered to come from similar species with different conformations or placed in different environments.

The 480 nm absorption could initially be considered to correspond to the quinonoid structure that usually absorbs at around 500 nm. However, the fluorescence excitation spectrum for this band showed a broad band ranging between 450 and 500 nm (Figure 5B) and is different from the narrow peak typical for the quinonoid structure. Therefore, we consider that the 480 nm absorption is not the quinonoid intermediate and may be related to the 430 nm absorption, which is thought to be the ketoenamine tautomeric species.

The absorption at 360−380 nm is generally ascribed to the deprotonated Schiff base. The absorption spectrum of D315N, however, does not essentially change with pH. This indicates that the 360−380 nm absorption band of D315N does not come from the deprotonated Schiff base. Again, we consider that this species may be related to the 340 nm absorption, which is interpreted to be the enolimine tautomeric species. That the fluorescence excitation spectra (Figure 5B) showed smooth curves and had no spikes observed for the absorption spectra (Figure 4) indicates that these spikes arise from minor impurities that are difficult to remove and that the absorption bands are largely those of PLP derivatives. From these considerations, we adopt the interpretation that the multiple absorption bands arise from a limited number of PLP species placed at different environments.

For many PLP enzymes, excitation of the enolimine species of the Schiff base results in emission at around 500 nm, identical to that of the emission caused by the excitation of the ketoenamine species, in addition to the emission around 390 nm. The ~500 nm emission comes from a species generated by the migration of the proton from O3′ (enolimine) to the imine N (ketoenamine) in the excited state, and the ~390 nm emission is the direct emission of the enolimine in the excited state before migration of the proton.[34] The wild-type HDC shows little emission at 500 nm on excitation of the enolimine species.[4] In the D315N mutant, however, no emission at around 500 nm was seen upon excitation of the 360 nm absorption species, although the ~500 nm emission is clearly seen upon excitation of the 430 and/or 480 nm absorption bands.

In summary, the results obtained with this mutant allow us to suggest that the D315N mutation could strongly alter the status of the PLP Schiff base in the active site, as indicated by the possible existence of ketoenamine and enolimine species placed in multiple microenvironments, lack of the large Stokes shift on excitation of the enolimine species caused by the proton migration in the excited state, and the shift in tautomeric equilibrium toward the ketoenamine form reflecting a decrease in polarity in its microenvironment. Altogether, we consider that the mutation of the D315 residue should indeed distort the optimum conformation of K308 and the polarity of its environment, thereby decreasing the efficiency of the initial Schiff base formation, as well as the following steps necessary to further the reaction and release the products.

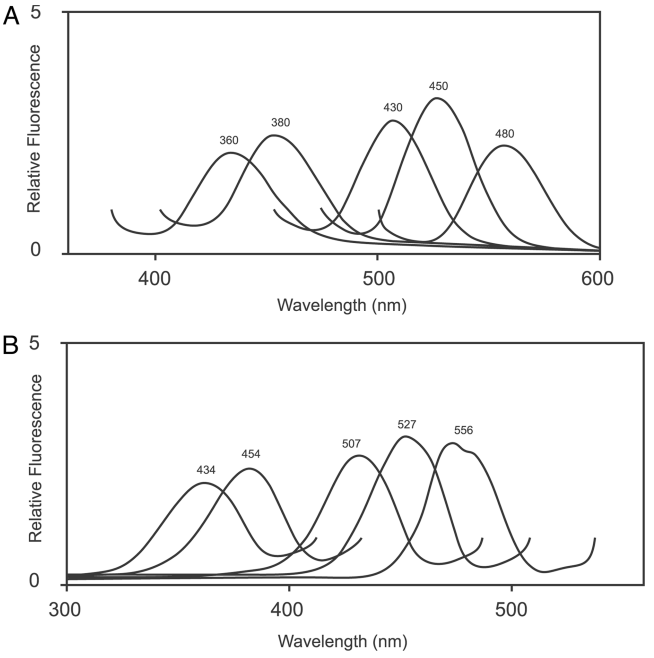

Figure 5. Fluorescence spectra of the mutant version D315N. (A) Fluorescence emission spectra. Excitation wavelengths are indicated on the different peaks. (B) Fluorescence excitation spectra of the peaks shown in panel A. Emission values are indicated on the respective excitation peaks.

3.5. Comparison among Homologous PLP-Dependent Decarboxylases Allows Us to Suggest New Applications for the Present Findings. To investigate the putative existence of a similar ionic arrangement in other evolutionary enzymes, we initially carried out multiple sequence alignments, including HDCs and DDCs from different living organisms and mammalian GADs. An alignment of representative sequences is shown in Figure 6. Curiously, in mammalian GADs, the D315 homologous position is occupied by a Q residue. As mentioned before, an amide group at this position caused the inactivation of mammalian HDC. Following our hypothesis on the role of the electrostatic hotspot interaction as one of the major structural determinants of mammalian HDC dimerization, the differences observed in the alignment should be accompanied by important differences in the quaternary structural organization of Gram-negative HDCs and GADs with respect to mammalian HDCs and DDCs. In fact, some of the bacterial HDCs have been described as tetrameric enzymes.[35,36] Some GAD enzymes have been found to be hexameric enzymes.[37] To avoid speculation, we do not do any further structural comparison with bacterial and plant PLP-dependent HDCs, or with GADs. However, the present data should provide valuable information for those groups working on the structural characterization of these other related enzymes, which control biogenic amine and alkaloid synthesis in many different organisms where they also play important physiological roles.

In any case, it is tempting to think that synthesis of specific ligands of this ionic motif could constitute a novel possibility for selective intervention of PLP-dependent HDC activities because dimerization (more specifically, the negative charge of the D315 carboxylate group) is critical for the proper conformation of the catalytic site of animal HDC. For instance, this strategy could allow us to inhibit, in a selective manner, animal HDC versus the same enzyme from other sources. This possibility would be relevant, as such a selective inhibition cannot yet be reached by using other previously characterized inhibitors that have the PLP-dependent HDC catalytic center as the target. In fact, HDC from both Gram-negative bacteria and animal sources can coexist

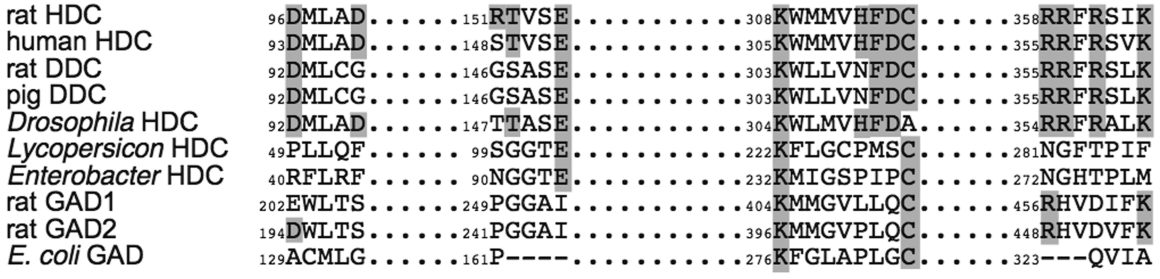

Figure 6. Alignment of fragments homologous to those of rat HDC that contain the ionic residues mentioned in the text. In boxes, the most relevant rat HDC residues mentioned in the text and their identical counterparts in other homologous L-aaDCs are highlighted. The first residues of each homologous fragment are numbered for each protein.

in the same physiological system (for instance, in the gastrointestinal track).

On the other hand, it is noteworthy that a similar but larger electrostatic hotspot is also observed in the X-ray structure of pig DDC. This electrostatic hotspot involves the following ionic residues of both DDC monomers: D92, E150, D310, R356, and R358, which are exactly the counterparts of D96, E155, R359, and R361 in rat HDC (Figure 6). Therefore, HDC and DDC also seem to share this dimerization motif, as occurs with other structural and functional characteristics. It has been suggested that the side chain of D310 of DDC could establish hydrogen bonds important for the right conformation of the K303-containing loop.[38] The occurrence of these hydrogen bonds is indeed supported by our work. Nevertheless, the present work shows that the role of D315, or its counterparts in the other homologous enzymes, is more drastic than a simple local structural distortion of weak electrostatic interactions, as the lack of these carboxylate groups could also affect the whole arrangement of the dimerization interface and the dynamics of these surfaces, which has been demonstrated to occur, at least during HDC reaction.

The electrostatic hotspot studied here adds to other structural and functional parallelisms between mammalian HDC and DDC, including sequence identity, tautomeric forms of the holoenzyme, and quaternary structure. But there are also slight structural differences that lead finally to important functional differences between both enzymes. These include the higher catalytic efficiency and less stringent substrate specificity of the latter when compared to mammalian HDCs. The slight differences between them could be responsible for any functional differences, and testing this hypothesis would need further work. In any case, the present results should also be of interest for groups working on the molecular bases of dopamine and serotonin synthesis. As far as we know, this structural characteristic of DDC has not been mentioned so far.

4. CONCLUDING REMARKS

The present work was designed to analyze the dimer interface of mammalian HDC. The enzyme prevents direct interaction between the electrostatic hotspots of both monomers because they are in a mainly hydrophobic dimerization surface and show electrostatic repulsion. Some of the ionic residues participating in the hotspot (especially D315) are located just in between the two catalytic sites, establishing an electropositive environment that can anchor PLP to each active site. In addition to the most exposed charged moieties, other thiol and hydroxyl groups and charged residues can contribute to the stabilization of the polar patch. It is tempting to hypothesize that this part of the protein could suffer rearrangements during the different stages of the reactions, thereby contributing to the conformational change that has been previously observed from biophysical approaches. These findings can provide valuable information for the full characterization of this poorly understood mammalian enzyme and also for DDC, an enzyme producing other biogenic amines that also has physiological and pharmacological importance. This ionic motif does not seem to be shared by other PLP-dependent L-aaDCs, such as the bacterial PLP-dependent HDC, providing insight for developing selective inhibitors that are able to distinguish between these two enzymes sharing both substrates and cofactors.

AUTHOR INFORMATION

Corresponding Author

*Phone: +34-952131674. Fax: +34-952132000. E-mail: kika@uma.es.

Present Addresses

[⊥]Department of Medicine, Veterans Affairs McGuire Medical Center/Virginia Commonwealth University, Richmond, Virginia 23249, United States.

Author Contributions

[∥]Both authors have contributed equally to the present work.

ACKNOWLEDGMENT

The authors thank Dr. Ignacio Tuñón and Dr. Javier Ruiz-Pernía from Universitat de València and Dr. Sergio Martí from Universitat Jaume I for their valuable advice and computational support. This work was supported by Grant SAF2008-2522 (Ministerio de Ciencia e Innovación, Spain), Grant BIO-267 from Junta de Andalucía, and funds from Fundación Ramón-Areces. CIBERER is an initiative of the ISCIII.

ABBREVIATIONS

3D, three-dimensional; DDC, aromatic L-amino acid decarboxylase or DOPA decarboxylase (EC 4.1.1.28); DOPA, L-3,4-dihydroxyphenylalanine; GAD, glutamate decarboxylase (EC 4.1.1.15); HDC, histidine decarboxylase (EC 4.1.1.22); HisOMe, histidine methyl ester; L-aaDCs, L-amino acid decarboxylases; MD, molecular dynamics; PLP, pyridoxal 5′-phosphate; rms, root-mean-square deviations; UV/vis, ultraviolet/visible

REFERENCES

(1) Ohmori, E.; Fukui, T.; Imanishi, N.; Yatsunami, K.; Ichikawa, A. *J. Biochem. (Tokyo)* **1990**, *107*, 834–9.
(2) Taguchi, Y.; Watanabe, T.; Kubota, H.; Hayashi, H.; Wada, H. *J. Biol. Chem.* **1984**, *259*, 5214–21.
(3) Fleming, J. V.; Wang, T. C. *J. Biol. Chem.* **2003**, *278*, 686–94.
(4) Olmo, M. T.; Sanchez-Jimenez, F.; Medina, M. A.; Hayashi, H. *J. Biochem. (Tokyo)* **2002**, *132*, 433–9.
(5) Moya-Garcia, A. A.; Ruiz-Pernia, J.; Marti, S.; Sanchez-Jimenez, F.; Tunon, I. *J. Biol. Chem.* **2008**, *283*, 12393–401.
(6) Rodriguez-Caso, C.; Rodriguez-Agudo, D.; Moya-Garcia, A. A.; Fajardo, I.; Medina, M. A.; Subramaniam, V.; Sanchez-Jimenez, F. *Eur. J. Biochem.* **2003**, *270*, 4376–87.
(7) Ghosh, A. K.; Hirasawa, N.; Ohtsu, H.; Watanabe, T.; Ohuchi, K. *J. Exp. Med.* **2002**, *195*, 973–82.
(8) Graff, L.; Frungieri, M.; Zanner, R.; Pohlinger, A.; Prinz, C.; Gratzl, M. *Am. J. Pathol.* **2002**, *160*, 1561–5.
(9) Nathan, C. *Nature* **2002**, *420*, 846–52.
(10) Medina, M. A.; Urdiales, J. L.; Rodriguez-Caso, C.; Ramirez, F. J.; Sanchez-Jimenez, F. *Crit. Rev. Biochem. Mol. Biol.* **2003**, *38*, 23–59.
(11) Pino-Angeles, A.; Morreale, A.; Negri, A.; Sanchez-Jimenez, F.; Moya-Garcia, A. A. *Proteins* **2010**, *78*, 154–61.
(12) DeLano, W. L. *The PyMOL Molecular Graphics System*; DeLano Scientific: San Carlos, CA, 2002.
(13) Kabsch, W.; Sander, C. *Biopolymers* **1983**, *22*, 2577–637.
(14) Dolinsky, T. J.; Nielsen, J. E.; McCammon, J. A.; Baker, N. A. *Nucleic Acids Res.* **2004**, *32*, W665–7.
(15) Li, H.; Robertson, A. D.; Jensen, J. H. *Proteins* **2005**, *61*, 704–21.
(16) Field, M. J. *A Practical Introduction to the Simulation of Molecular Systems*; Cambridge University Press: New York, 1999.

(17) Phillips, J. C.; Braun, R.; Wang, W.; Gumbart, J.; Tajkhorshid, E.; Villa, E.; Chipot, C.; Skeel, R. D.; Kalé, L.; Schulten, K. *J. Comput. Chem.* **2005**, *26*, 1781–1802.
(18) MacKerell, A. D.; Bashford, D.; Bellott; Dunbrack, R. L.; Evanseck, J. D.; Field, M. J.; Fischer, S.; Gao, J.; Guo, H.; Ha, S.; Joseph-McCarthy, D.; Kuchnir, L.; Kuczera, K.; Lau, F. T. K.; Mattos, C.; Michnick, S.; Ngo, T.; Nguyen, D. T.; Prodhom, B.; Reiher, W. E.; Roux, B.; Schlenkrich, M.; Smith, J. C.; Stote, R.; Straub, J.; Watanabe, M.; Wiórkiewicz-Kuczera, J.; Yin, D.; Karplus, M. *J. Phys. Chem. B* **1998**, *102*, 3586–3616.
(19) Fogolari, F.; Brigo, A.; Molinari, H. *J. Mol. Recognit.* **2002**, *15*, 377–92.
(20) Baker, N. A.; Sept, D.; Joseph, S.; Holst, M. J.; McCammon, J. A. *Proc. Natl. Acad. Sci. U. S. A.* **2001**, *98*, 10037–41.
(21) Sheinerman, F. B.; Norel, R.; Honig, B. *Curr. Opin. Struct. Biol.* **2000**, *10*, 153–9.
(22) Schutz, C. N.; Warshel, A. *Proteins* **2001**, *44*, 400–17.
(23) Karp, D. A.; Gittis, A. G.; Stahley, M. R.; Fitch, C. A.; Stites, W. E.; Garcia-Moreno, E. B. *Biophys. J.* **2007**, *92*, 2041–53.
(24) Sharp, K. A.; Honig, B. *Annu. Rev. Biophys. Biophys. Chem.* **1990**, *19*, 301–32.
(25) Engel, N.; Olmo, M. T.; Coleman, C. S.; Medina, M. A.; Pegg, A. E.; Sánchez-Jiménez, F. *Biochem. J.* **1996**, *320*, 365–8.
(26) Burkhard, P.; Dominici, P.; Borri-Voltattorni, C.; Jansonius, J. N.; Malashkevich, V. N. *Nat. Struct. Biol.* **2001**, *8*, 963–7.
(27) Hayashi, H.; Mizuguchi, H.; Kagamiyama, H. *Biochemistry* **1993**, *32*, 812–8.
(28) Nishino, J.; Hayashi, H.; Ishii, S.; Kagamiyama, H. *J. Biochem. (Tokyo)* **1997**, *121*, 604–11.
(29) Heifetz, A.; Katchalski-Katzir, E.; Eisenstein, M. *Protein Sci.* **2002**, *11*, 571–87 and references therein.
(30) Jones, S.; Thornton, J. M. *Proc. Natl. Acad. Sci. U. S. A.* **1996**, *93*, 13–20.
(31) Moya-Garcia, A. A.; Medina, M. A.; Sanchez-Jimenez, F. *Bioessays* **2005**, *27*, 57–63 and references therein.
(32) Dartsch, C.; Chen, D.; Persson, L. *Regul. Pept.* **1998**, *77*, 33–41.
(33) Metzler, C. M.; Harris, A. G.; Metzler, D. E. *Biochemistry* **1988**, *27*, 4923–33.
(34) Zhou, X.; Toney, M. D. *Biochemistry* **1999**, *38*, 311–20.
(35) Guirard, B. M.; Snell, E. E. *J. Bacteriol.* **1987**, *169*, 3963–8.
(36) Tahanejad, F. S.; Naderi-Manesh, H.; Habibinejad, B.; Mahmoudian, M. *Eur. J. Med. Chem.* **2000**, *35*, 567–76.
(37) Capitani, G.; Tramonti, A.; Bossa, F.; Grutter, M. G.; De Biase, D. *FEBS Lett.* **2003**, *554*, 41–4.
(38) Poupon, A.; Jebai, F.; Labesse, G.; Gros, F.; Thibault, J.; Mornon, J. P.; Krieger, M. *Proteins* **1999**, *37*, 191–203.